REGULAR ARTICLE

blood advances

# CD19.CAR T-cell–derived extracellular vesicles express CAR and kill leukemic cells, contributing to antineoplastic therapy

Paola Lanuti,[1,2] Francesco Guardalupi,[1,2] Giulia Corradi,[3] Rosalba Florio,[4] Davide Brocco,[5] Serena Veschi,[4] Elsa Pennese,[3] Domenico De Bellis,[1,2] Francesca D'Ascanio,[1,2,6] Anna Piro,[4] Laura De Lellis,[4] Pasquale Simeone,[1,2] Maria Concetta Cufaro,[2,4] Serena Pilato,[4,7] Isabella D'Amario,[1,2] Ida Villanova,[3] Barbara Di Francesco,[3] Lucia Di Re,[1,2,8] Fabio Verginelli,[2,4] Damiana Pieragostino,[2,8] Prassede Salutari,[3] Fabrizia Colasante,[3] Annalisa Natale,[3] Maria Vittoria Mattoli,[9] Simone Vespa,[1,2] Antonella Fontana,[4,7] Raffaella Giancola,[3] Bianca Fabi,[3] Stefano Baldoni,[3] Stella Santarone,[3] Francesco Restuccia,[1] Nicola Tinari,[5] Piero Del Boccio,[2,4] Alessandro Cama,[4] and Mauro Di Ianni[1-3]

[1]Department of Medicine and Aging Sciences and [2]Center for Advanced Studies and Technology, University of Chieti-Pescara, Chieti, Italy; [3]Department of Oncology and Hematology, Pescara Hospital, Pescara, Italy; [4]Department of Pharmacy and [5]Department of Medical, Oral and Biotechnological Sciences, G. d'Annunzio University of Chieti-Pescara, Chieti, Italy, [6]Department of Humanities, Law and Economics, Leonardo da Vinci University, Torrevecchia Teatina, Italy; [7]UdA-TechLab, Research Center and [8]Department of Innovative Technologies in Medicine and Odontoiatry, G. d'Annunzio University of Chieti-Pescara, Chieti, Italy; and [9]Department of Hospital Services, Nuclear Medicine Unit, Pescara Hospital, Pescara, Italy

**Key Points**

- CD19.CAR$^+$EVs represent a new dynamic biomarker of CAR T-cell activity and contribute to the direct killing of cancer targets.
- CD19.CAR$^+$EVs could be a new therapeutic tool for strengthening or even replacing CAR T-cell therapy.

Chimeric antigen receptor (CAR) T-cell–derived extracellular vesicles (EVs) might represent a new therapeutic tool for boosting CAR T-cell antileukemic effects. Here, a cohort of 22 patients who received infusion with CD19 CAR T cells were monitored for the presence of circulating CD19 CAR$^+$ T-cell–derived EVs (CD19.CAR$^+$EVs), which were then separated and functionally characterized for their killing abilities. A good manufacturing practice (GMP)-compliant separation method was also developed. Results demonstrated that CD19.CAR$^+$EVs were detectable in peripheral blood up to 2 years after infusion, indicating long-lasting persistence of their parental cells. Notably, early decreases of circulating CD19.CAR$^+$EV concentrations correlated with failure of CAR T-cell therapy. Circulating CD19.CAR$^+$EVs displayed a median size (standard deviation) of 133.1 ± 65.5 nm and carried a proapoptotic protein cargo. These EVs expressed higher CAR levels than their parental cells. Furthermore, CD19.CAR$^+$EVs did not activate heterologous T cells and produced significant, specific, and dose-dependent cytotoxic effects on CD19$^+$ cell lines and primary cells. The new GMP-compliant EV isolation method allowed for a recovery of 63% ± 5.7% of CD19.CAR$^+$EVs. A deeper analysis of the different protein cargoes carried by EVs derived from different CAR T-cell subpopulations identified a proapoptotic functional pathway linked to CD8$^+$LAG-3$^+$ EVs. Overall, our data indicate that CD19.CAR$^+$EVs may be proposed as promising dynamic new biomarkers of CAR T-cell activity and, by contributing to the direct killing of leukemic targets, represent a new product with strong therapeutic potential that could be infused independently of CAR T cells.



Submitted 18 September 2024; accepted 15 January 2025; prepublished online on *Blood Advances* First Edition 4 February 2025. https://doi.org/10.1182/bloodadvances.2024014860.

Original data are available on request from the corresponding author, Mauro Di Ianni (mauro.diianni@unich.it).

The full-text version of this article contains a data supplement.

## Introduction

Chimeric antigen receptor (CAR) T lymphocytes represent the most innovative form of immunotherapy against cancer, demonstrating particular success in the treatment of non-Hodgkin lymphomas,[1] B-cell acute lymphoblastic leukemia,[2,3] and multiple myeloma.[4]

Extracellular vesicles (EVs) are a heterogeneous population of membrane-surrounded particles, released by any cell type and carrying a variety of biological cargoes, such as RNAs, microRNAs, proteins, lipids, and DNA fragments. They play significant roles in the intracellular cross talk.[5,6] EVs have been traditionally classified into 3 main subsets, based on their biogenesis: exosomes, microvesicles, and apoptotic bodies.[7] Exosomes, typically of endosomal origin, are released by exocytosis, whereas microvesicles, also known as microparticles or ectosomes, bud directly from the plasma membrane of their parental cells, and apoptotic bodies are released during cell apoptosis processes.[8] Recently, new EV subtypes have been described; these include oncosomes, particularly large oncosomes, a distinct class of EVs ranging from 1 to 10 μm in diameter, that originate from the shedding of membrane blebs in cancer cells,[9] and migrasomes, vesicle-like structures that form on the retraction fibers of migrating cells and play significant roles in various biological processes.[10-12] These different EV subtypes display overlapping sizes and phenotypes; therefore, the EV subsetting, based on their biogenesis, is difficult to establish and is considered misleading.[13] For this reason, the International Society of Extracellular Vesicles endorsed the use of the term "EVs" for all EV subtypes, simplifying the EV classification on the basis of EV diameters. According to the International Society of Extracellular Vesicles, EVs are currently classified as small EVs (<200 nm) or medium/large EVs (>200 nm).[13,14]

EVs budded by T cells are membrane-bounded vesicles that act as powerful regulators of immunological responses, mediated both by their surface receptors and their content.[15] CAR T-cell–derived EVs (CAR$^+$EVs) have been underlined for their potential as a new therapeutic tool in cancer immunotherapy.[16,17] It is known that CAR$^+$EVs express CARs on their surface and carry high levels of cytotoxic molecules (ie, perforin and granzyme B).[18,19] Therefore, CAR$^+$EVs display significant antitumor effects, interacting with their target cells, in which they deliver their cytotoxic cargo, enhancing the overall antitumor immune response and increasing the therapeutic efficacy of CAR T cells in vivo.[17,20-22] CAR$^+$EVs exhibit a lower risk of toxic effects than CAR T-cell therapy, circumventing safety concerns associated with live cell therapies, potentially minimizing the risk of adverse events and immune-related toxicities.[18,23] This is due to their nonproliferative nature, which helps them evade immunosuppressive mechanisms and to control the administered dose.[18,23-25] EVs are released in the extracellular space and are widely studied as promising dynamic biomarkers for liquid biopsy purposes.[26-29] Higher levels of circulating CAR$^+$EVs released by CD19 CAR$^+$ T cells were shown to predict immune effector cell–associated neurotoxicity syndrome in patients with B-cell lymphomas.[30] Here, we undertook the task of deeply studying the role of circulating biomarkers and the potential of new therapeutics of CD19 CAR$^+$EVs (CD19.CAR$^+$EVs). We demonstrated that CD19.CAR$^+$EVs remained detectable in peripheral blood (PB) of patients for up to 2 years after infusion, overwhelming the disappearance of their parental cells that occurred ~1 year after infusion. Blood concentration of these EVs had an early decrease in nonresponding patients, suggesting a role of CD19.CAR$^+$EVs as prognostic biomarkers. Furthermore, these EVs carried a proapoptotic cargo and displayed significant in vitro cytotoxic abilities, suggesting that they may also participate in antitumor surveillance, representing a new promising therapeutic tool for strengthening or even replacing CAR T-cell therapies.

## Methods

### Patients

Twenty-two patients (13 with large B-cell lymphomas, 3 mantle cell lymphoma, 2 primary mediastinal B-cell lymphoma, and 4 acute lymphoblastic leukemia), receiving tisa-cel (n = 4), axi-cel (n = 11), or brexu-cel (n = 7), were enrolled between January 2022 and July 2024. The study was approved by the local ethical committee (RA/0404367) and was performed following the Helsinki Declaration; written informed consent was obtained from all participants. Clinical results and patient characteristics are summarized in supplemental Tables 1-3.

### CAR T-cell monitoring by flow cytometry and droplet digital polymerase chain reaction

Flow cytometry and digital droplet polymerase chain reaction (PCR) for CD19 CAR$^+$ T-cell detection were performed as detailed in supplemental Methods and supplemental Figure 1A. CD19 CAR$^+$ T cells and their subsets were also isolated as described in supplemental Methods.

### Flow cytometry EV analysis

PB or cell supernatant samples were stained to detect CD19.CAR$^+$EVs as already described.[31-34] Briefly, 5 μL of PB added to 200 μL of PBS 1× or 100 μL of CAR$^+$ T-cell–derived supernatant added to 100 μL of PBS 1× were stained, as detailed in supplemental Table 4 (monitoring/fluorescence-activated cell sorting [FACS] sorting panel), for 45 minutes in the dark at room temperature (RT). For intravesicular staining of EVs, samples were further fixed and permeabilized using 200 μL of Cytofix/Cytoperm (Becton Dickinson Biosciences) for 20 minutes in the dark at RT and stained with flotillin-1, perforin, or granzyme B antibodies for 30 minutes (supplemental Table 4, EV characterization panel). Samples were acquired by flow cytometry and analyzed for EV concentrations, phenotypes, and molecules of equivalent fluorochrome (MEFs), as described and detailed in supplemental Methods.[31,33,35] The gating strategy used to identify CD19.CAR$^+$EVs is depicted in supplemental Figure 1B.

The limit of detection of the flow cytometry EV analysis (132 nm) was assessed according to current guidelines (see supplemental Methods for protocol details).[36]

### Isolation and concentration of EVs for their characterization and functional assay assessment

Supernatants of FACS-isolated CD19 CAR$^+$ T cells (from preinfusion bags or circulating PB samples) were isolated for further characterization and functional assay assessment. Briefly, cell supernatants were concentrated by tangential flow filtration, which preserves all EV sizes in the retentate, and then EVs were isolated by FACS as previously described.[31,37] FACS-isolated EVs were finally concentrated by polyethylene glycol precipitation or ultracentrifugation for further characterization and functional assays. These procedures are detailed in supplemental Methods.

### Isolation of EVs by immunomagnetic separation

A new protocol based on CD3$^+$ immunomagnetic selection of EVs was optimized (supplemental Methods).

### EV characterization

All isolated EV samples were analyzed by nanoparticle tracking analysis (NTA), transmission electron microscopy, atomic force microscopy (AFM), western blot, and proteomics, as previously described.[28,38-40] These procedures are detailed in supplemental Methods.

### EV functional assays

CD19.CAR$^+$EV cytolytic activity was assayed both by MTT and flow cytometry 7-aminoactinomycin D (7-AAD) incorporation, using Raji and SUP-B15 cell lines as targets. Briefly, the MTT assay was performed using different protein doses (0, 0.0025, 0.005, 0.01, and 0.015 µg per target cell) of circulating CD19.CAR$^+$EVs or CD19.CAR$^+$EVs obtained from CD19 CAR T-cell bags (pre-infusion CD19.CAR$^+$EVs) to treat cell targets, as detailed in supplemental Methods. The highest CD19.CAR$^+$EV protein dose (0.015 µg protein per target cell) produced a significant target cell inhibition and was used to study the flow cytometry 7-AAD incorporation after 24 hours of treatment, as detailed in supplemental Methods. The percentage of EV-induced killing was calculated based on the 7-AAD$^+$ gate, using the following formula:

$$\text{Killing (\%)} = [1 - \text{viable target cells (sample)} \,/\, \text{viable target cells (control)}] \times 100\%$$

### Statistical analysis

Statistical analyses were performed using GraphPad Prism software version 10.2.0. A $P$ value <.05 was considered significant. For each experiment, the used test was specified in the related figure legend.

## Results

### Characterization of CD19 CAR$^+$ T-cell phenotypes

Across all analyzed samples from the infused bags, CD19 CAR$^+$ T cells were highly represented, averaging 70.64% (standard error of the mean [SEM], 4.57) of CD3$^+$ T cells (supplemental Figure 2A). CD4 frequencies were significantly higher (62.01%; SEM, 2.66) than those of CD8 (35.12%; SEM, 3.18; $P = .0018$; supplemental Figure 2A). The assessment of T-cell subsets unveiled distinct frequencies, with naïve T cells displaying a mean of 4.67% (SEM, 1.63), central memory T cells 30.84% (SEM, 6.95), effector memory T cells 51.67% (SEM, 7.67), and effector memory re-expressing CD45RA T cells 2.65% (SEM, 0.70; supplemental Figure 2B).

### CD19 CAR$^+$ T-cell and EV monitoring

As shown in Figure 1, the persistence of CAR T cells after their infusion was monitored at different time points for 2 years, both by flow cytometry and droplet digital polymerase chain reaction (ddPCR). In parallel, the circulating concentration of CD19.CAR$^+$EVs was analyzed (Figure 1), using the gating strategy detailed in supplemental Figure 1B. As shown in Figure 1, the concentrations of CAR$^+$ T cells analyzed by flow cytometry and ddPCR were significantly correlated throughout the monitoring ($r = .9728$; $P < .0001$). Of note, CD19.CAR$^+$EV concentrations were significantly higher than those of their circulating parental cells from day +1 to the end of the monitoring ($P < .0001$), both when CAR T cells were analyzed by flow cytometry or ddPCR (except day +7). Overall, these results showed the early appearance of circulating CD19.CAR$^+$EVs (day +1), overwhelming the disappearance of circulating parental cells and remaining detectable even after 2 years from the infusion (Figure 1). Notably, a 2-way analysis of variance performed across all analyzed time points revealed no significant differences in terms of CD19.CAR$^+$EV concentrations among the 3 CAR T-cell infusion products (axi-cel, tisa-cel, and brexu-cel; $P > .05$). Furthermore, when we compared the concentration of circulating EVs at different time points, we observed that CD19.CAR$^+$EVs significantly decreased relative to day +1 in nonresponders (day +21, $P = .0340$; day +35, $P = .0444$), whereas they remained stable in responders (Figure 1; supplemental Table 5). Pretreatment tumor burden did not correlate with the concentration of circulating EVs both in responders ($R^2 = .0107$; $P = .8073$) and nonresponders ($R^2 = .0107$; $P = .8073$). Considering the limited half-life of CAR$^+$EVs (~90% were reported to be cleared within 5 minutes[16]), CAR T cells persisting in the body out of blood circulation are the only conceivable source of circulating CAR$^+$EVs, which persist for

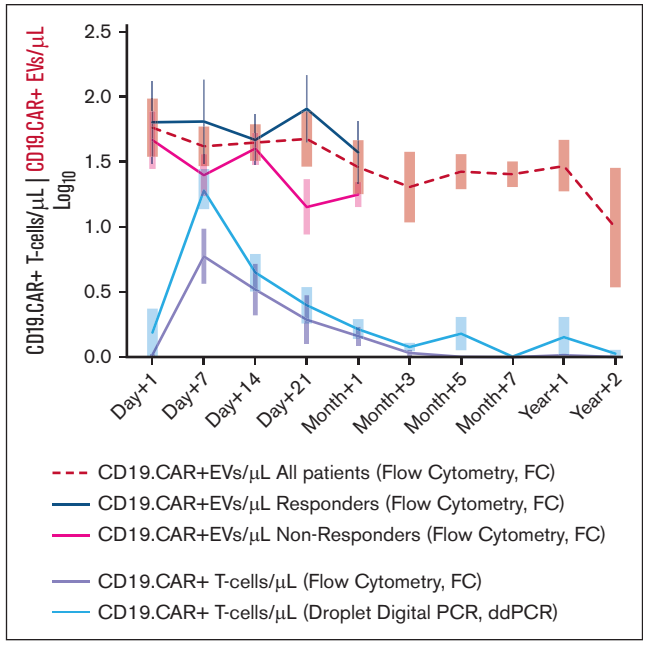


**Figure 1. Monitoring of CD19 CAR T cells and CD19.CAR$^+$EVs in patients treated with CD19 CAR T cells.** A total of 22 patients were monitored for 2 years from CD19 CAR T-cell infusion. The concentration of circulating CD19 CAR T cells was monitored both by flow cytometry (purple line) and ddPCR (blue line). CD19 CAR T-cell monitoring was paralleled with the concentration of CD19.CAR$^+$EVs (red line). Flow cytometry analysis of CD19.CAR$^+$EVs in responding vs nonresponding patients is also shown. Data were log transformed. A 2-way analysis of variance (ANOVA), followed by Tukey multiple comparisons test, was performed. An alpha value of .05 was established for the significance threshold. Each time point represents the mean (+SEM) of at least 3 independent measurements from distinct patients. Data are represented as mean + SEM; Mann-Whitney nonparametric test, and Robust Regression followed by OUTlier Identification test for outliers were applied.

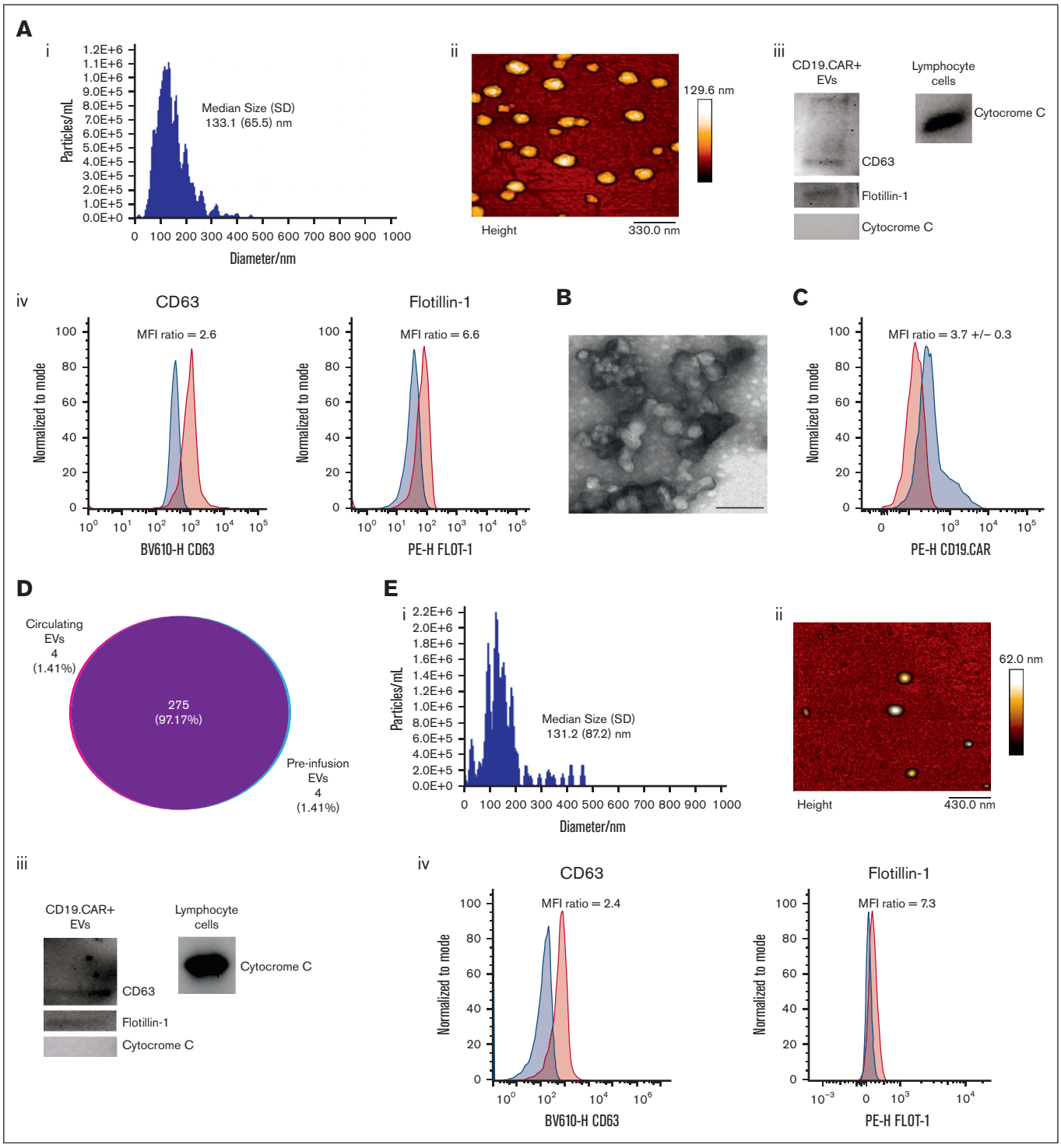


**Figure 2. Characterization of CD19.CAR$^+$EVs.** (A) NTA (i); AFM analysis of circulating CD19.CAR$^+$EVs (ii); western blot analysis of CD63, flotillin-1, and cytochrome C in circulating CD19.CAR$^+$EV samples (T lymphocytes were used as controls for cytochrome C expression) (iii); and flow cytometry evaluation of CD63 and flotillin-1 expression in circulating CD19.CAR$^+$EVs (iv). CD63 and flotillin-1 expression (red histograms) were analyzed using the related fluorescence minus one (FMO) as controls (blue histograms). Mean fluorescence intensity (MFI) ratio values were calculated by dividing the MFI of the positive sample and that of the related FMO control. Data are representative of 3 separate experiments. (B) Transmission electron microscopy analysis of circulating CD19.CAR$^+$EVs (scale bar, 100 nm). (C) Flow cytometry evaluation of CAR expression on circulating CD19.CAR$^+$EVs. CAR expression (red histogram) was analyzed using the related FMOs as controls (blue histogram). MFI ratio values were calculated by dividing the MFI of the positive sample and that of the related FMO control. Data are representative of 3 separate experiments. (D) Venn diagram shows the common and uncommon proteins identified in circulating and preinfusion CD19.CAR$^+$EVs. Same amount of EVs (pool of 3 individuals per condition containing $3 \times 10^6$ EVs) were compared when proteomic analyses were performed to parallel circulating vs preinfusion EV cargoes. The number 4 refers to the number of identified proteins (4, corresponding to the 1.41% of the total number of

at least 2 years. Indeed, our data indirectly demonstrate, to our knowledge, for the first time in patients, the persistence of CAR$^+$EVs throughout our follow-up that lasted 2 years. Notably, supporting this finding, flow cytometry analysis of the bone marrow from patients with acute lymphoblastic leukemia or mantle cell lymphoma with marrow involvement showed that CAR T cells were still present in these tissue samples after their disappearance from circulation (3.5% ± 1.4% vs 0). These results suggest a role of CAR$^+$EVs as new promising dynamic biomarkers of CAR T-cell persistence and efficacy, deserving validation in larger and more extended future studies analyzing distinct hematologic malignancies.

## Characterization of CD19.CAR$^+$EVs

To deeply characterize EVs stemming from preinfusion and circulating CAR T cells, both CAR T-cell populations were isolated from preinfusion bags (n = 3) or from PB samples of patients who received infusion (n = 22), respectively. Purified CD19.CAR$^+$EV samples were further analyzed for their morphological features as well as for the expression of typical EV markers.[13,14] Results from NTA measurements of circulating CD19.CAR$^+$EVs revealed that they displayed diameters in the range of small EVs (median size, 133.1 nm; standard deviation [SD], ±65.5 nm; Figure 2Ai), in line with previously reported data.[18] Parallel transmission electron microscopy (Figure 2B) and AFM (Figure 2Aii) data showed that these EVs displayed characteristic round/spherical shapes, and their diameters (AFM mean diameter, 103.5 nm; SD, ±32.3 nm; Figure 2Aii) overlapped with those measured by NTA. A further characterization of EV markers was performed both by western blot and flow cytometry, and according to current guidelines, 2 positive and 1 negative EV markers were studied.[13,14] As shown in Figure 2Aiii, circulating CD19.CAR$^+$EVs expressed CD63 and the cytosolic flotillin-1 protein, whereas, as required, they did not express cytochrome C, which was detected on T cells used as positive controls. The EV expression of CD63 and flotillin-1 was confirmed and corroborated by flow cytometry (Figure 2Aiv). Overlapping results, in terms of sizes (preinfusion EV median size, 131.2 nm; SD, +87.2 nm), shapes, and phenotypic features, were obtained when preinfusion CD19.CAR$^+$EVs were analyzed (Figure 2Ei-iv). The entire population of CD19.CAR$^+$EVs expressed the CAR (Figure 2C). Further proteomic analyses showed a 97.1 % overlap among proteins carried by circulating and preinfusion CD19.CAR$^+$EVs (Figure 2D). In addition, according to STRING, proteins identified in circulating and preinfusion CD19.CAR$^+$EVs were involved in the "EV" pathway (gene ontology cellular component, 0070062; false discovery rate, 1.22e-92), further confirming the EV origin of the protein data set (supplemental Table 6). Therefore, circulating and preinfusion CD19.CAR$^+$EVs, stemming from CD19 CAR T cells, display similar features.

## Killing abilities of CD19 CAR$^+$ T cells and derived EVs

To ascertain the cytolytic potential of preinfusion and circulating CD19 CAR$^+$ T cells, 2 CD19$^+$ cell lines (Raji and SUP-B15) were used as targets (supplemental Figure 3A). As expected, CAR T cells efficiently killed Raji and SUB-B15 cells in a dose-dependent manner, as shown in supplemental Figure 3B-C.

The cytolytic abilities of CD19.CAR$^+$EVs were then studied using the same CD19$^+$ cell lines as targets. As shown in Figure 3A, a dose-response MTT analysis was conducted by treating Raji (Figure 3Ai) or SUP-B15 cell lines (Figure 3Aii) with growing doses of circulating EVs (expressed as microgram of EV proteins per target cell). Results showed that, after 48 hours of treatment, CD19.CAR$^+$EVs significantly affected the cell viability of both tested cell lines in a dose-dependent manner. The percentage of viable cells at the highest tested dose (0.015 μg of EV proteins per target cell) was 27.7% ± 5.51% for Raji and 39.9% ± 7.11% for SUP-B15 cell lines. These data were further confirmed using 0.015-μg proteins of circulating and preinfusion EV proteins per target cell to treat the same cell lines and analyzing the cell 7-AAD incorporation by flow cytometry after 24 hours of treatment. We observed that both circulating (Figure 3B) and preinfusion (Figure 3C) CD19.CAR$^+$EVs exerted a significant cytolytic activity, reaching a killing percentage of 20.3% (±3.8%) and 37.8% (±7.0%) when Raji and SUP-B15 were used as targets, respectively (Figure 3B), whereas the killing percentage induced by preinfusion CD19.CAR$^+$EVs was 42.0% (±12.3%) and 35.8% (±13.8%) for Raji and SUP-B15, respectively (Figure 3C). These data were further confirmed using primary CD19$^+$ blasts as targets. As evidenced in Figure 3C, CD19.CAR$^+$EVs significantly affect target viability, reaching a killing percentage of 18.8% + 9.8%.

The evidenced cytolytic effects of CD19.CAR$^+$EVs were specific, given that the same assay performed using EVs stemming from proliferating heterologous T cells did not affect target cell viability, either in CD19$^+$ cell lines (killing [percent], 0.71% ± 2.19%) or primary CD19$^+$ primary blasts (killing percent, 2.35% ± 1.91%). Furthermore, CD19.CAR$^+$EVs were also used to treat carboxyfluorescein succinimidyl ester-stained heterologous T cells. As shown in Figure 3D, 24 hours of 0.015-μg CD19.CAR$^+$EV protein treatment did not activate heterologous T cells, indicating a potential off-the-shelf application of these EVs.

Moreover, the analysis of expressed molecules of CAR by MEF (Figure 4A) was performed both on circulating CD19.CAR$^+$EVs and their parental cells from the same patients (n = 3). Red bar represents the estimated MEFs per μm$^2$ of the CAR$^+$EV surface, whereas the blue bar represents the estimated MEFs per μm$^2$ of the CAR T-cell surface. CD19.CAR$^+$EVs express a higher CAR density on their surfaces than their parental cells (Figure 4A). We then analyzed the cargo of CD19.CAR$^+$EVs. As shown in Figure 4B, all detected EVs carried perforin and granzyme B. The protein cargo identified by proteomics in both preinfusion and circulating EVs was analyzed by ingenuity pathway analysis software. Data show that circulating CD19.CAR$^+$EVs (Figure 4C) carry 116 of 279 identified proteins associated with the function "apoptosis" ($P = 1.26 \times 10^{-16}$). The same function was activated by 117 of 279 identified proteins carried by preinfusion CD19.CAR$^+$EVs (Figure 4D; $P = 4.27 \times 10^{-17}$).

**Figure 2 (continued)** identified proteins) uniquely carried by circulating EVs, whereas 275 proteins (99.97 % of identified proteins) were those shared by circulating and preinfusion CAR$^+$EVs, and 4 other proteins (1.41% of identified proteins) were carried only by preinfusion CAR$^+$EVs. (E) NTA (i) and AFM analysis (ii) of preinfusion CD19.CAR$^+$EVs; western blot analysis of CD63, flotillin-1, and cytochrome C in preinfusion CD19.CAR$^+$EV samples (T lymphocytes were used as controls for cytochrome C expression) (iii); and flow cytometry evaluation of CD63 and flotillin-1 expression in preinfusion CD19.CAR$^+$EVs (iv). CD63 and flotillin-1 expression (red histograms) were analyzed using the related FMOs as controls (blue histograms). MFI ratio values were calculated by dividing the MFI of the positive sample and that of the related FMO control. Data are representative of 3 separate experiments.

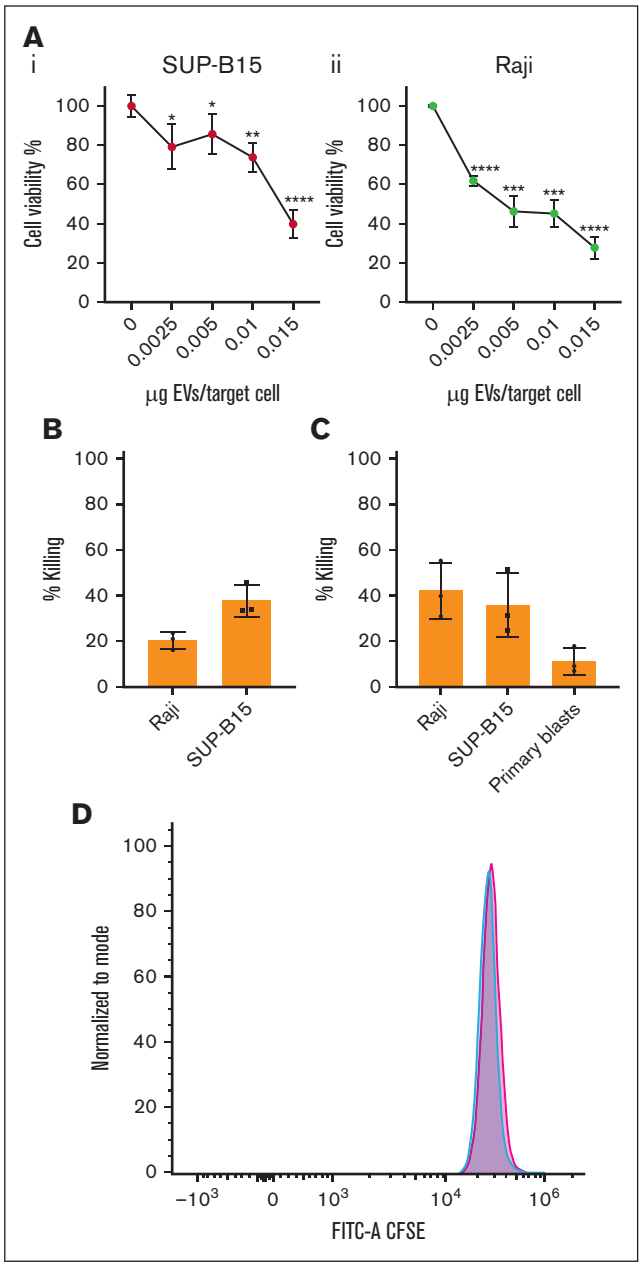


**Figure 3. In vitro cytolytic activity of CD19.CAR$^+$EVs on Raji and SUP-B15 cell lines.** (A) Cell viability of 2 cell lines, Raji (i) and SUP-B15 (ii), assessed by MTT assays after incubation for 48 hours with CD19.CAR$^+$EVs at the indicated concentrations. Data shown are means ± SD of 3 to 4 replicates. *Statistically significant differences, compared with control (0 μg); *$P < .05$; **$P < .01$; ***$P < .001$; ****$P < .0001$. (B) Flow cytometry killing assays were performed using the concentration of 0.015 μg of circulating EVs per target cell to treat both Raji and SUP-B15 cell lines and analyzing their cytolytic activity by measuring the 7-AAD staining of target cells after 24 hours of treatment (Student *t* test, $P = .0187$). Values are averages of 3 independent experiments. (C) Flow cytometry killing assays were performed using the concentration of 0.015 μg of preinfusion EVs per target cell to treat both Raji and SUP-B15 cell lines and analyzing their cytolytic activity by measuring the 7-AAD staining of target cells after 24 hours of treatment (Student *t* test, not significant). (D) The immunogenicity of CD19.CAR$^+$EVs was studied by treating heterologous T cells for 24 hours with the same dose of CD19.CAR$^+$EVs used for testing their cytolytic abilities (0.015-μg protein EV per target cell). The red histogram represents the CFSE profile of untreated heterologous T cells, whereas the overlaid blue histogram represents the CFSE profile of heterologous T cells treated with CD19.CAR$^+$EVs. Data are representative of 2 independent experiments. CFSE, carboxyfluorescein succinimidyl ester.

Altogether, these data suggest that CD19.CAR$^+$EVs express high CAR levels and carry molecules capable of activating the lysis of the targets.

## CD19 CAR$^+$ T-cell subtypes and their derived EVs

We further characterized the phenotype of the infused CD19 CAR T cells by analyzing the expression of different markers known to regulate the exhaustion of T cells, that is, PD-1, LAG-3, and TIM-3 (Figure 5A). Interestingly, we found that PD-1 is more expressed in CD4$^+$ than in CD8$^+$ CAR$^+$ T cells (mean ± SEM; CD3, 45.10% ± 5.65%; CD4, 54.52% ± 6.47%; CD8, 27.39% ± 5.50%; CD4 vs CD8, $P = .0100$), whereas the expression of LAG-3 is higher in CD8$^+$ than in CD4$^+$ CAR$^+$ T cells (mean ± SEM; CD3, 19.17% ± 4.55%; CD4, 9.22% ± 2.88%; CD8, 30.23% ± 7.41%; CD4 vs CD8, $P = .0386$). The expression of TIM-3 did not change between CD3$^+$, CD4$^+$, and CD8$^+$ CAR$^+$ T cells (Figure 5A). Next, CD4$^+$PD-1$^+$ and CD8$^+$LAG-3$^+$ CAR$^+$ T cells were isolated by FACS to perform cytotoxicity assays using a CD19$^+$ cell line (Raji) as the target. Interestingly, we found that the expression of PD-1 on CD4$^+$ CAR$^+$ T cells did not alter their cytotoxic potential (Figure 5B). Similarly, CD8$^+$LAG-3$^+$ CAR$^+$ T cells displayed a higher ability to kill tumor cells than total CD3$^+$ CAR$^+$ T cells (mean ± SEM; CD3$^+$ CAR$^+$ T cells, 53.51% ± 4.31%; CD8$^+$LAG-3$^+$ CAR$^+$ T cells, 77.31% ± 6.45%; $P = .0115$; Figure 5B). The comparison of the frequencies of CD4$^+$PD1$^+$ and CD8$^+$LAG3$^+$ CAR$^+$ T-cell subpopulations at day +14 (Figure 5C) showed stable trends, without statistical differences ($P > .05$) with respect to preinfused CAR$^+$ T-cell subsets. Indeed, for CD4$^+$PD1$^+$ CAR$^+$ T cells, the initial mean percentage was 40.70% (SEM, ±5.06%), which remained substantially stable (41.21%; SEM, ±6.92%) at day +14 (adjusted $P = .9953$). Similarly, for CD8$^+$LAG3$^+$ CAR$^+$ T cells, the initial mean percentage was 8.83% (SEM, ±2.32%), which did not vary significantly at day +14 (5.86%; SEM, ±2.08%; adjusted $P = .9946$). Given the already demonstrated cytolytic potential of CD19.CAR$^+$EVs, we undertook the task to study the protein cargo of the EVs released from each of the studied subtypes, to understand their contribution to overall cytolytic activity. As reported in Figure 5D, the protein expression of LAG3$^+$ EVs, compared with LAG3$^-$ EVs, showed a significant activation of apoptotic functional pathway as a downstream effect, suggesting a greater contribution of LAG3$^+$ EVs in the cytolytic activity ($P = 2.73 \times 10^{-28}$; z score, 2.149).

## Optimization of CD19.CAR$^+$EV isolation under good manufacturing practice-compliant conditions

Considering the evidence that CD19.CAR$^+$EVs might have therapeutic potential, we explored the efficacy of an isolation method that may be easily implemented for good manufacturing practice (GMP) applications. In this regard, we optimized CD19.CAR$^+$EV immunomagnetic separation using anti-CD3 magnetic beads, reaching a recovery of 63% ± 5.7%. Indeed, GMP anti-CD3 magnetic beads are already commercially available and used in clinical settings.[41] As shown in Figure 6A-B, CD3–immune-selected CD19.CAR$^+$EVs displayed diameters (median size + SD;

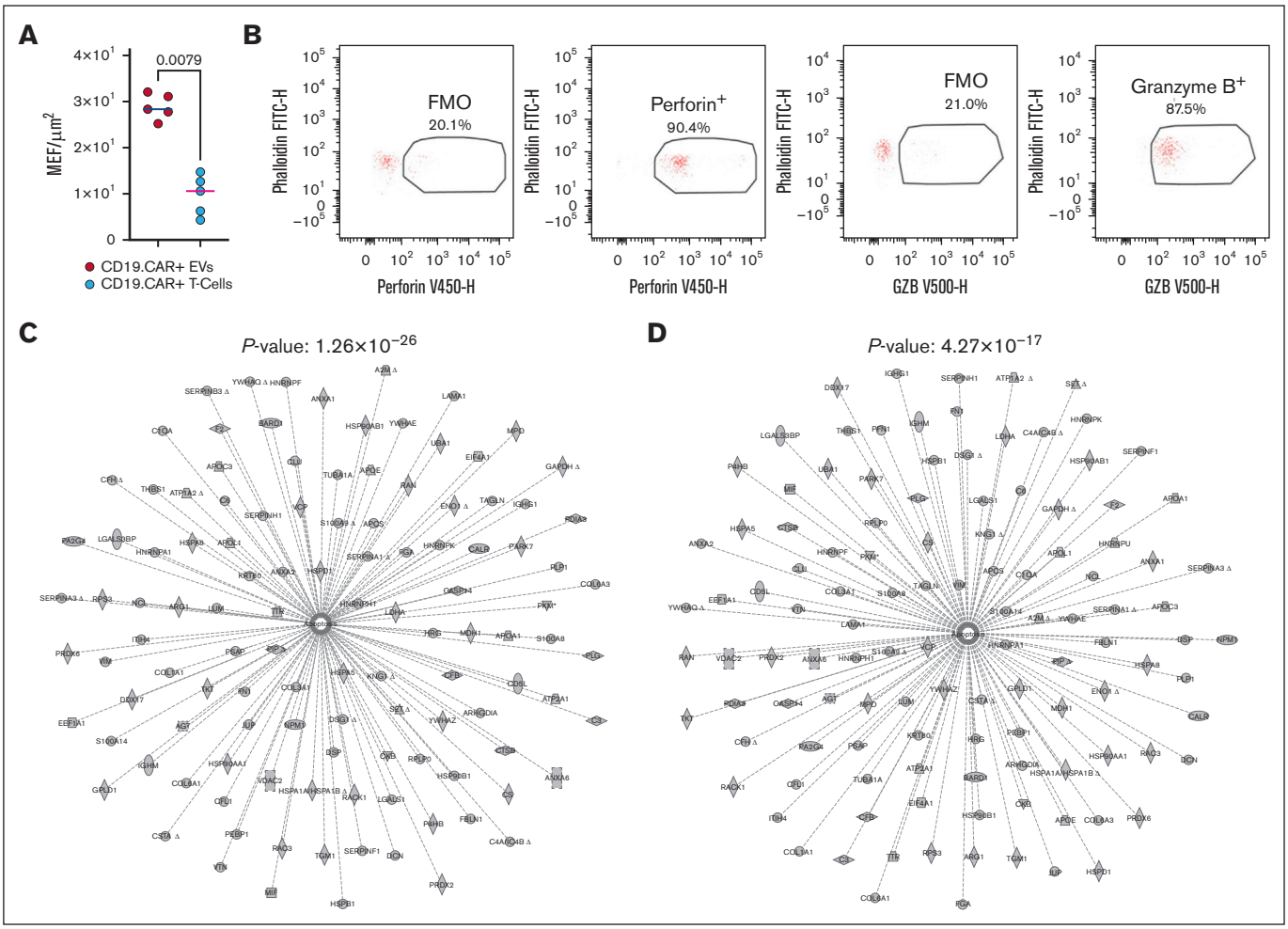


**Figure 4. CD19.CAR$^+$EV protein cargo.** (A) Estimated MEFs per μm$^2$. The analysis of MEF was performed both on circulating CD19.CAR$^+$EVs and their circulating parental cells from the same patients (n = 3). The red dots refer to the estimated MEFs per μm$^2$ of CD19.CAR$^+$EV surface, whereas the blue dots represents the estimated MEFs per μm$^2$ of CAR T-cell surface. (B) Dot plots showing expression of granzyme B and perforin in circulating CD19.CAR$^+$EVs; the fluorescence minus one (FMO) control for granzyme B is shown (i); the percentage of granzyme B–positive EVs is represented (mean percent, 61.9% [SD, 4.7%]; mean MFI ratio, 3.5 [SD, 0.8]) (ii); the control FMO of perforin is shown (iii); and the percentage of perforin-positive EVs is represented (mean percent, 67.6% [SD, 4.2%]; mean MFI ratio, 6.7 [SD, 1.3]) (iv). The protein functional analyses of circulating (C) and preinfusion CD19.CAR$^+$EVs (D), calculated by IPA with all identified proteins, are shown. IPA, ingenuity pathway analysis.

NTA analysis, 103.3 + 55.7 nm, Figure 6A; AFM analysis, 90.7 + 39.2 nm, Figure 6B) and shapes overlapping with those isolated by FACS. Furthermore, they express CD63 and flotillin-1 (Figure 6C). CD3–immune-selected CD19.CAR$^+$EVs also displayed significant killing abilities (Figure 6D). We observed that CD19 CAR$^+$ T cells release ~3.5 EVs per parental cells in 12 hours in vitro, and each CD19.CAR$^+$EVs carries 0.0005 μg of proteins. Considering that the number of CAR$^+$ T cells in each bag ranges from ~6 × 10$^7$ to 2 × 10$^8$ cells, a range of 1.2 × 10$^8$ to 6 × 10$^8$ EVs (equivalent to 6 × 10$^4$ to 3 × 10$^5$ μg of EVs) can be obtained from each donor. Furthermore, according to the detected concentrations of circulating CD19.CAR$^+$EVs (Figure 1), their total amount in 5 liters of each patient PB would be in the range 8.5 × 10$^7$ to 5 × 10$^8$, corresponding to ~4 × 10$^4$ to 2.5 × 10$^5$ μg of EVs. We also observed that their circulating concentrations remained stable for at least 2 years (Figure 1); therefore, hypothesizing that their cytolytic functions in vivo overlap with those observed in vitro, it is conceivable that these concentrations of circulating CD19.CAR$^+$EVs theoretically kill 2.7 × 10$^{11}$ to 1.67 × 10$^{13}$ tumor cells every 24 hours.

## Discussion

CAR T-cell therapy recently gained great attention because of its outstanding efficacy in the management of several B-cell malignancies. Among the alternative and intriguing therapeutic avenues linked to CAR T cells, their derived EVs have garnered great attention due to their safer profile and potential to replicate CAR T-cell functions, possibly addressing drawbacks inherent in conventional CAR T-cell therapy.[17,42] Furthermore, monitoring CD19.CAR$^+$EVs provides a potential noninvasive method for dynamically evaluating CAR T-cell functions and persistence in patients. Here, we undertook the task of characterizing preinfusion bag contents in terms of CAR T cells and their derived EVs. We further studied the pattern of circulating CAR T-cell elements (cells

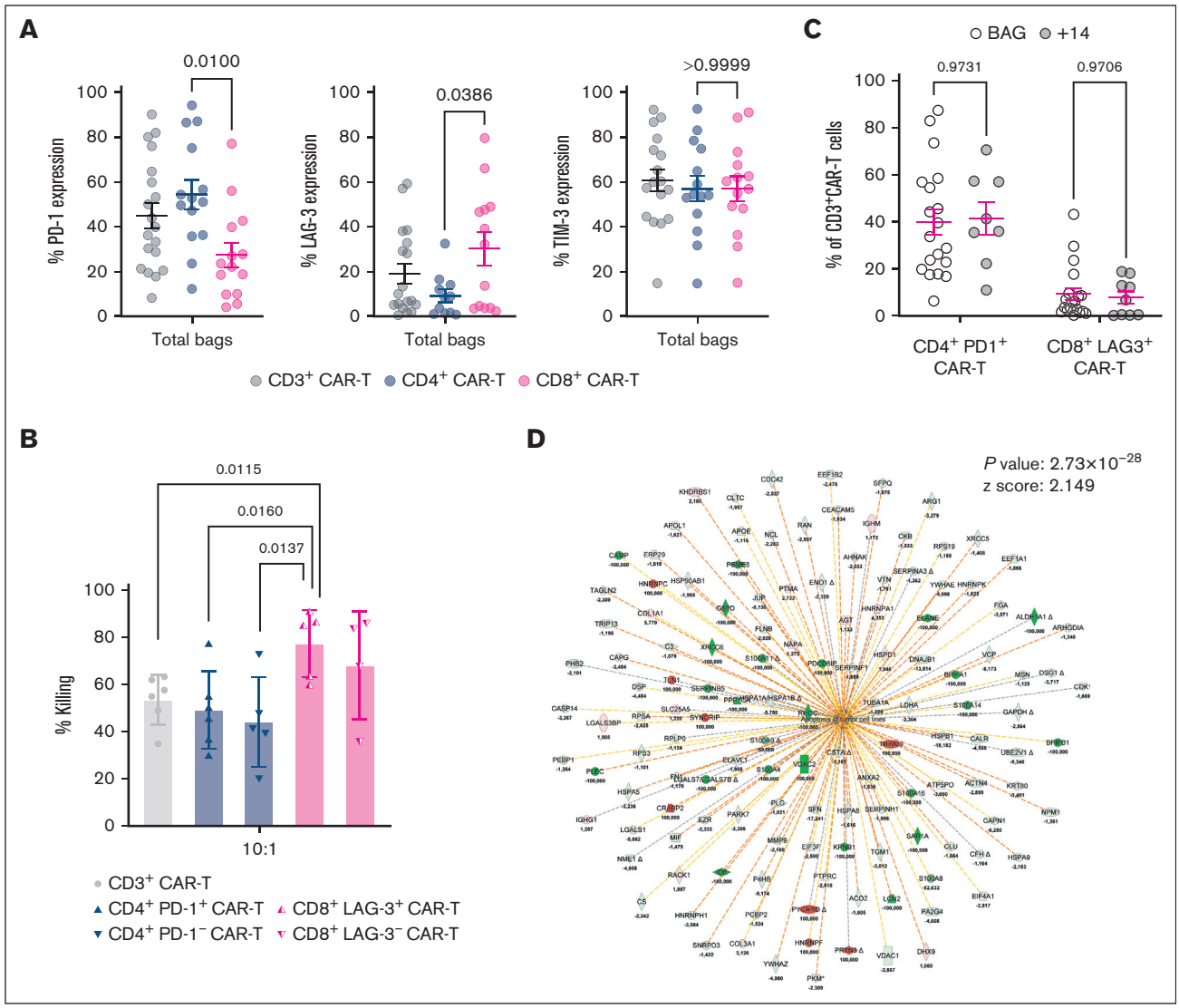


**Figure 5. CD19 CAR T-cell–expressing PD-1 and LAG-3 are functional and produce EVs.** (A) Flow cytometry analysis of markers, known to be involved in T-cell exhaustion, expressed on CD19 CAR T cells, residual from the infusion bags. The 3 graphs indicate the percentage of PD-1$^+$ cells, LAG-3$^+$ cells, and TIM-3$^+$ cells gated on total CD3$^+$ CAR T cells (gray circles), CD4$^+$ CAR T cells (blue circles), and CD8$^+$ CAR T cells (blue circles). Data are presented as mean ± SEM (1-way ANOVA; CD4$^+$PD-1$^+$ CAR T cells vs CD8$^+$PD-1$^+$ CAR T cells, $P = .0100$; CD4$^+$LAG-3$^+$ CAR T cells vs CD8$^+$LAG-3$^+$ CAR T cells, $P = .0386$). (B) Cytotoxic function of total CD3$^+$ CAR T cells, CD4$^+$PD-1$^+$ CAR T cells, CD4$^+$PD-1$^-$ CAR T cells, CD8$^+$LAG-3$^+$ CAR T cells, and CD8$^+$LAG-3$^-$ CAR T cells, isolated by FACS from the infusion bag, against a CD19-expressing cell line, Raji. After 24 hours of culture, the percentage of target living cells with CAR T cells (target-to-CAR T-cell ratio, 1:10) was assessed by flow cytometry. The bars represent the mean and SEM of killing of CAR T cells derived from at least 4 different donors. (Student *t* test; CD3$^+$ CAR T cells vs CD8$^+$LAG-3$^+$ CAR T cells, $P = .0115$; CD4$^+$PD-1$^+$ CAR T cells vs CD8$^+$LAG-3$^+$ CAR T cells, $P = .0160$; CD4$^+$PD-1$^-$ CAR T cells vs CD8$^+$LAG-3$^+$ CAR T cells, $P = .0137$). (C) Comparison of the percentage of CD4$^+$PD-1$^+$ CAR T cells and CD8$^+$LAG-3$^+$ CAR T cells, assessed by flow cytometry. The cells analyzed were obtained from the residual bags or from the PB of patients, 14 days after CD19 CAR T-cell infusion (2-way ANOVA, not significant). (D) The protein functional analysis calculated by ingenuity pathway analysis with all identified proteins is shown for CD8$^+$LAG3$^+$ EVs paralleled with the CD8$^+$LAG-3$^-$ EV compartment.

and EVs) up to 2 years after CAR T-cell infusion. We noticed that circulating CD19.CAR$^+$EVs appear early after CD19.CAR T-cell infusion (day +1), confirming previously reported data.[43] Intriguingly, their concentrations remained higher than those of CD19 CAR T parental cells throughout monitoring, overwhelming the disappearance of circulating parental cells (1 year after infusion) and remaining detectable even 2 years after infusion.

These data confirm, in patients, the evidence previously obtained in xenograft models, showing that CAR T cells are not seen in circulating blood at later time points but persist for some time in the body, outside the blood circulation.[7,44-47] Indeed, CAR$^+$EVs are rapidly cleared from circulation[16]; therefore, our data, showing their long-lasting persistence in PB, together with the findings evidencing the bone marrow homing of CAR T cells once they

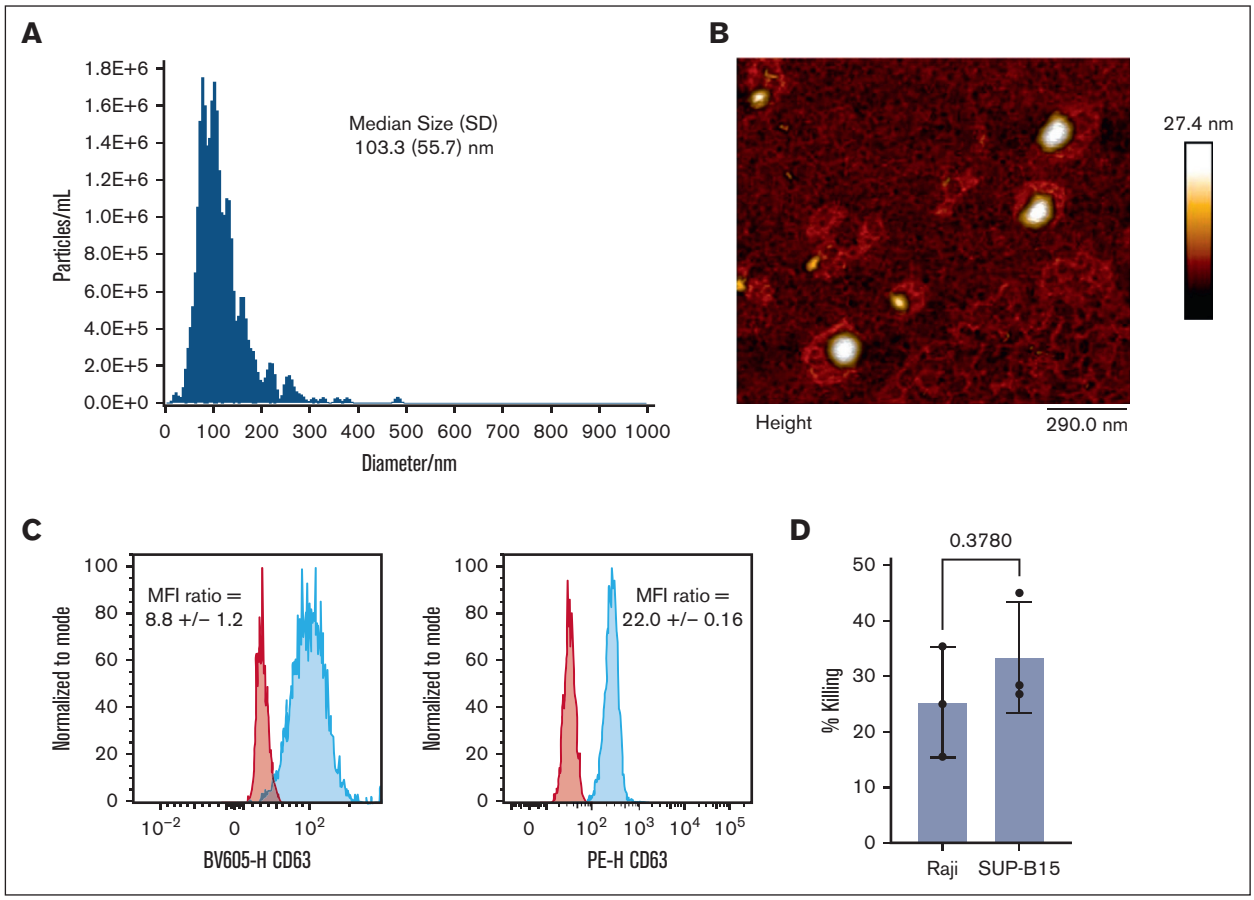


**Figure 6. Characterization of CD3$^+$–immune-selected CD19.CAR$^+$EVs.** NTA (A) and AFM analysis (B). (C) Flow cytometry evaluation of CD63 and flotillin-1 expression. CD63 and flotillin-1 expression (red histograms) were analyzed using the related FMOs as controls (blue histograms). MFI ratio values were calculated by dividing the MFI of the positive sample and that of the related FMO control. Data are representative of 3 separate experiments. (D) Flow cytometry killing assays were performed using the concentration of 0.015 μg of protein from CD3-immunoselected EVs per target cell to treat both Raji and SUP-B15 cell lines and by analyzing their cytolytic activity by measuring the 7-AAD staining of target cells after 24 hours of treatment.

disappear from circulation, indicate that their parental CAR T cells persist in the body of patients who underwent infusion, outside the blood circulation, for at least 2 years. Notably, the long persistence of infused CAR T cells is one of the clinically relevant results that our data demonstrate, to our knowledge, for the first time in patients, indicating that circulating CAR$^+$EVs may serve as a marker of CAR T-cell persistence outside PB.

More interestingly, we further undertook the task of studying the features and the cytolytic potential of both preinfusion and circulating CD19.CAR$^+$EVs, with the aim of understanding whether they have the potential to contribute to the efficacy of CAR T-cell therapies. For these reasons, we analyzed the features of CD19.CAR$^+$EVs contained in preinfusion CAR T-cell products and paralleled them with those of circulating CD19.CAR$^+$EVs, demonstrating that these 2 CD19.CAR$^+$EV subsets overlap in terms of size, shape, and protein cargo and even in inducing significant cytotoxic, dose-dependent effects on their targets. Overall, these data showed that CD19.CAR$^+$EVs retain morphological and functional characteristics in vivo. It is already known that CD19.CAR$^+$EVs express CARs on their surface, enabling targeted action against tumor cells.[18] Here, we not only confirmed the CAR expression on EVs derived from CD19 CAR$^+$ T cells, but we also observed, to our knowledge, for the first time, that CD19.CAR$^+$EVs expressed higher levels of CARs than their parental cells, as indicated by measurements of MEFs per μm$^2$ of CAR T-cell surface. On the contrary, we observed that both analyzed populations of CD19.CAR$^+$EVs (preinfusion and circulating) contain typical cytotoxic molecules, including perforin and granzyme B. In line with their parental cells, the main CD19.CAR$^+$EV mechanism of action has been linked to the granzyme/perforin system.[18] On the contrary, as shown by our group and in a previous study,[18] there is a specific target killing by EVs derived from CAR$^+$ vs EVs derived from nontransduced T cells, indicating that surface expression of CAR is essential for targeting of EVs and their killing activity. Furthermore, as shown in CAR T cells,[48] a higher or lower density of CAR molecules present on the surface of EVs is expected to influence the docking efficiency of EVs on their targets. Therefore, retaining the antigen specificity of their parental cells,[49] CD19.CAR$^+$EVs allow for targeted therapy against tumor-associated antigens.[17,18,21,50] In addition, the calculated amount of circulating EVs, based on our data, was shown to kill $2.7 \times 10^{11}$ to $1.67 \times 10^{13}$ tumor cells every 24 hours, which amounts to a substantial killing of tumor cells, considering that effective levels of CD19.CAR$^+$EVs are sustained for at least 2 years.

These data underline that CD19.CAR$^+$EVs represent a promising new product with a strong therapeutic potential that could be possibly infused independently of CAR T cells. In such a context, it should be noted that EVs display unique biodistribution capabilities and safety profiles, they cross biological barriers, delivering therapeutic molecules to target sites, and are insensitive to PD-L1 inhibition,[18] offering clear advantages over their parental cells or synthetic drug delivery systems.[51,52] These data are corroborated by results from a previous study demonstrating CAR$^+$EV effectiveness in vivo.[18] That study showed that CAR$^+$EVs armed with CARs designed against different antigenic targets have potent antitumor effects and low toxicity in mouse models representative of several malignancies.[18]

It is also known that T-cell receptor activation induces the production of cytotoxic T cell-derived EVs expressing the T-cell receptor/CD3ζ complex.[53] Therefore, CD19.CAR$^+$EVs are direct attackers of B-cell malignancies. Although the correlation between exhaustion markers of the apheretic product and the poor or lower functionality of lymphocytes is clear,[54] postinfusion functional studies on patient samples are scarce. A correlation has been demonstrated between an increased number of circulating CD4$^+$PD1$^+$LAG3$^+$ CAR T cells and improved outcomes.[55] Here, we were able to separate circulating CD4$^+$PD1$^+$ and CD8$^+$LAG3$^+$ CAR T cells, demonstrating their killing capacity on CD19$^+$ target cells. Furthermore, we characterized the respective EVs, demonstrating a significant activation of apoptotic functional pathway as a downstream effect. These results open up the possibility for future studies on EV subpopulations and their possible clinical use. Even if some EV subtypes (ie, tumor-derived and platelet-derived EVs) may modulate immune responses,[6,28,49,56-61] as already known for mesenchymal-derived EVs, displaying reduced immunogenic properties,[62,63] we confirmed that CD19.CAR$^+$EVs do not activate heterologous T cells. Therefore, CD19.CAR$^+$EVs have the potential to be an "off-the-shelf product,"[18] and the translation of these findings from preclinical and early-stage studies to clinical practice, leveraging the benefits of both CAR T cells and EVs to enhance therapeutic efficacy while mitigating associated risks, has the potential to open new routes for the assessment of novel immunotherapies. It must be noted that, despite their potential, the clinical application of CD19.CAR$^+$EVs faces several challenges; among them, the optimization of GMP-compliant procedures, ensuring productions of consistent quality and quantity, is essential.[64,65] Here, we optimized the use of a GMP grade, scalable method, based on the isolation of EVs by anti-CD3 immunomagnetic beads, which could be used for future clinical applications. We successfully demonstrated that EVs isolated by anti-CD3 immunomagnetic beads from CD19 CAR T cells overlap in terms of features and functions with those isolated by standard procedures, preserving the EV biological integrity. Such a procedure is efficient (63% ± 5.7% of recovery) and quick, and it can be fully automated and adapted for commercial closed-system setups, enabling easy upscaling for clinical applications.

In summary, our results suggest that CD19.CAR$^+$EVs may serve as biomarkers for monitoring CAR T-cell persistence and efficacy, predicting the outcomes of CAR T-cell therapy. We also show that CD19.CAR$^+$EVs have the potential to provide a substantial contribution to CAR T-cell therapy, offering a promising and scalable approach for cancer immunotherapy, which combines the advantages of CAR T cells with the benefits of cell-free therapies. In conclusion, our study indicates that CD19.CAR$^+$EVs have the potential to open a new approach to more effective and safer cancer treatments.

## Acknowledgments

This study was supported by the European Union (EU)–NextGenerationEU under the National Recovery and Resilience Plan (NRRP), Mission 4 Component 2 (M4C2 Investment 1.4), Call for Tender number 3138, dated 16 December 2021, funded by Italian Ministry of University (award number, CN_00000041) for the project titled "National Center for Gene Therapy and Drugs based on RNA Technology." The Concession Degree number 1035, dated 17 June 2022, was adopted by the Italian Ministry of University (Codice Unico di Progetto: D73C22000810006 [P.L., A.C., and M.D.I. (Principal Investigator)]), which also support the junior researcher positions of D.B., R.F., and P. Simeone. The junior researcher position of P. Simeone is funded by the European Union–NextGenerationEU under the NRRP Mission 4 Component 2 (M4C2 Investment 1.5), Call for Tender number 3277, dated 30 December 2021, by the Italian Ministry of University (award number, ECS00000041) for the project titled "Innovation, digitalization and sustainability for the diffused economy in Central Italy." The Concession Degree number 1057, dated 23 June 2022, was adopted by the Italian Ministry of University (Codice Unico di Progetto: D73C22000840006). The PhD fellowship of D.D.B. (code number 1353889) has been funded within the framework of Programma Operativo Nazionale RI 2014/2020, I.1 "Innovative PhDs with industrial characterization," by the Italian Ministry of University and Research, Italy, Fondo Sociale Europeo-Fondo Europeo di Sviluppo Regionale. This work was supported by the Associazione Italiana contro le Leucemie-Linfomi e Mieloma, L'Aquila Section, and Pescara Section, Italy.

## Authorship

Contribution: P.L., F.V., D.P., N.T., P.D.B., A.C., and M.D.I. designed the study, oversaw the results, and drafted the manuscript; F.G., G.C., R.F., D.B., and A.F. contributed to the design and interpretation of the study; E.P., P. Salutari, F.C., A.N., M.V.M., and S.S. provided clinical data; and F.R., F.G., G.C., R.F., D.B., S. Veschi, D.D.B., F.D., A.P., L.D.L., P. Simeone, M.C.C., S.P., I.D., I.V., B.D.F., L.D.R., R.G., B.F., S. Vespa, and S.B. performed the in vitro studies and interpreted the results.

Conflict-of-interest disclosure: The authors declare no competing financial interests.

ORCID profiles: G.C., 0000-0003-2585-4881; R.F., 0000-0002-3095-1451; D.B., 0000-0001-8634-7184; S. Veschi, 0000-0003-0450-9210; D.D.B., 0000-0002-0953-1989; F.D., 0000-0002-0588-5536; A.P., 0009-0000-8076-2491; L.D.L., 0000-0002-6460-2508; M.C.C., 0000-0002-6457-7795; F.V., 0000-0002-8636-2517; D.P., 0000-0003-1015-3484; P.S., 0009-0006-0064-5951; S. Vespa, 0000-0001-6146-9302; A.F., 0000-0002-5391-7520; B.F., 0000-0002-1290-2760; S.B., 0000-0002-5420-5672; F.R., 0000-0002-4583-651X; P.D.B., 0000-0003-1653-2194; A.C., 0000-0003-3647-1368; M.D.I., 0000-0002-6701-4023.

Correspondence: Mauro Di Ianni, Department of Medicine and Aging Sciences, University of Chieti-Pescara, via Vetoio, 66100 Chieti, Italy; email: mauro.diianni@unich.it.

## References


1. Neelapu SS, Locke FL, Bartlett NL, et al. Axicabtagene ciloleucel CAR T-cell therapy in refractory large B-cell lymphoma. *N Engl J Med*. 2017;377(26):2531-2544.
2. Maude SL, Laetsch TW, Buechner J, et al. Tisagenlecleucel in children and young adults with B-cell lymphoblastic leukemia. *N Engl J Med*. 2018;378(5):439-448.
3. Grupp SA, Kalos M, Barrett D, et al. Chimeric antigen receptor-modified T cells for acute lymphoid leukemia. *N Engl J Med*. 2013;368(16):1509-1518.
4. Sharma P, Kanapuru B, George B, et al. FDA approval summary: idecabtagene vicleucel for relapsed or refractory multiple myeloma. *Clin Cancer Res*. 2022;28(9):1759-1764.
5. Dellar ER, Hill C, Melling GE, Carter DRF, Baena-Lopez LA. Unpacking extracellular vesicles: RNA cargo loading and function. *J Extracell Biol*. 2022;1(5):e40.
6. Marcoux G, Laroche A, Hasse S, et al. Platelet EVs contain an active proteasome involved in protein processing for antigen presentation via MHC-I molecules. *Blood*. 2021;138(25):2607-2620.
7. Catitti G, De Bellis D, Vespa S, Simeone P, Canonico B, Lanuti P. Extracellular vesicles as players in the anti-inflammatory inter-cellular crosstalk induced by exercise training. *Int J Mol Sci*. 2022;23(22):14098.
8. Simeone P, Bologna G, Lanuti P, et al. Extracellular vesicles as signaling mediators and disease biomarkers across biological barriers. *Int J Mol Sci*. 2020;21(7):2514.
9. Ciardiello C, Leone A, Lanuti P, et al. Large oncosomes overexpressing integrin alpha-V promote prostate cancer adhesion and invasion via AKT activation. *J Exp Clin Cancer Res*. 2019;38(1):317.
10. Fan C, Shi X, Zhao K, et al. Cell migration orchestrates migrasome formation by shaping retraction fibers. *J Cell Biol*. 2022;221(4):e202109168.
11. Zhai Z, Liu B, Yu L. The roles of migrasome in development. *Cell Insight*. 2024;3(1):100142.
12. Tan X, He S, Wang F, Li L, Wang W. Migrasome, a novel organelle, differs from exosomes. *Biochem Biophys Rep*. 2023;35:101500.
13. Thery C, Witwer KW, Aikawa E, et al. Minimal information for studies of extracellular vesicles 2018 (MISEV2018): a position statement of the International Society for Extracellular Vesicles and update of the MISEV2014 guidelines. *J Extracell Vesicles*. 2018;7(1):1535750.
14. Welsh JA, Goberdhan DCI, O'Driscoll L, et al. Minimal information for studies of extracellular vesicles (MISEV2023): from basic to advanced approaches [published correction appears in *J Extracell Vesicles*. 2024;13(5):e12451]. *J Extracell Vesicles*. 2024;13(2):e12404.
15. Yanez-Mo M, Siljander PR, Andreu Z, et al. Biological properties of extracellular vesicles and their physiological functions. *J Extracell Vesicles*. 2015;4(1):27066.
16. Tang XJ, Sun XY, Huang KM, et al. Therapeutic potential of CAR-T cell-derived exosomes: a cell-free modality for targeted cancer therapy. *Oncotarget*. 2015;6(42):44179-44190.
17. Pagotto S, Simeone P, Brocco D, et al. CAR-T-derived extracellular vesicles: a promising development of CAR-T anti-tumor therapy. *Cancers (Basel)*. 2023;15(4):1052.
18. Fu W, Lei C, Liu S, et al. CAR exosomes derived from effector CAR-T cells have potent antitumour effects and low toxicity. *Nat Commun*. 2019;10(1):4355.
19. Sadowski K, Olejarz W, Basak G. Modern advances in CARs therapy and creating a new approach to future treatment. *Int J Mol Sci*. 2022;23(23):15006.
20. Calvo V, Izquierdo M. T lymphocyte and CAR-T cell-derived extracellular vesicles and their applications in cancer therapy. *Cells*. 2022;11(5):790.
21. Aharon A, Horn G, Bar-Lev TH, et al. Extracellular vesicles derived from chimeric antigen receptor-T cells: a potential therapy for cancer. *Hum Gene Ther*. 2021;32(19-20):1224-1241.
22. Zhang Y, Ge T, Huang M, et al. Extracellular vesicles expressing CD19 antigen improve expansion and efficacy of CD19-targeted CAR-T cells. *Int J Nanomedicine*. 2023;18:49-63.
23. Wang C, Fu W, Lei C, Hu S. Generation and functional characterization of CAR exosomes. *Methods Cell Biol*. 2022;167:123-131.
24. Ding Y, Wang L, Li H, et al. Application of lipid nanovesicle drug delivery system in cancer immunotherapy. *J Nanobiotechnology*. 2022;20(1):214.
25. Sani F, Shojaei S, Tabatabaei SA, et al. CAR-T cell-derived exosomes: a new perspective for cancer therapy. *Stem Cell Res Ther*. 2024;15(1):174.
26. Brocco D, De Bellis D, Di Marino P, et al. High blood concentration of leukocyte-derived extracellular vesicles is predictive of favorable clinical outcomes in patients with pancreatic cancer: results from a multicenter prospective study. *Cancers (Basel)*. 2022;14(19):4748.
27. Brocco D, Simeone P, Buca D, et al. Blood circulating CD133+ extracellular vesicles predict clinical outcomes in patients with metastatic colorectal cancer. *Cancers (Basel)*. 2022;14(5):1357.
28. Piro A, Cufaro MC, Lanuti P, et al. Exploring the immunomodulatory potential of pancreatic cancer-derived extracellular vesicles through proteomic and functional analyses. *Cancers (Basel)*. 2024;16(10):1795.
29. Brocco D, Lanuti P, Pieragostino D, et al. Phenotypic and proteomic analysis identifies hallmarks of blood circulating extracellular vesicles in NSCLC responders to immune checkpoint inhibitors. *Cancers (Basel)*. 2021;13(4):585.

30. Storci G, De Felice F, Ricci F, et al. CAR+ extracellular vesicles predict ICANS in patients with B cell lymphomas treated with CD19-directed CAR T cells. *J Clin Invest*. 2024;134(14):e173096.

31. Marchisio M, Simeone P, Bologna G, et al. Flow cytometry analysis of circulating extracellular vesicle subtypes from fresh peripheral blood samples. *Int J Mol Sci*. 2020;22(1):48.

32. Falasca K, Lanuti P, Ucciferri C, et al. Circulating extracellular vesicles as new inflammation marker in HIV infection. *AIDS*. 2021;35(4):595-604.

33. Simeone P, Celia C, Bologna G, et al. Diameters and fluorescence calibration for extracellular vesicle analyses by flow cytometry. *Int J Mol Sci*. 2020;21(21):7885.

34. Efthymakis K, Bologna G, Simeone P, et al. Circulating extracellular vesicles are increased in newly diagnosed celiac disease patients. *Nutrients*. 2022;15(1):71.

35. Cossarizza A, Chang HD, Radbruch A, et al. Guidelines for the use of flow cytometry and cell sorting in immunological studies (second edition). *Eur J Immunol*. 2019;49(10):1457-1973.

36. Welsh JA, Arkesteijn GJA, Bremer M, et al. A compendium of single extracellular vesicle flow cytometry. *J Extracell Vesicles*. 2023;12(2):e12299.

37. Visan KS, Lobb RJ, Ham S, et al. Comparative analysis of tangential flow filtration and ultracentrifugation, both combined with subsequent size exclusion chromatography, for the isolation of small extracellular vesicles. *J Extracell Vesicles*. 2022;11(9):e12266.

38. Rossi C, Cicalini I, Cufaro MC, et al. Multi-omics approach for studying tears in treatment-naive glaucoma patients. *Int J Mol Sci*. 2019;20(16):4029.

39. Pieragostino D, Lanuti P, Cicalini I, et al. Proteomics characterization of extracellular vesicles sorted by flow cytometry reveals a disease-specific molecular cross-talk from cerebrospinal fluid and tears in multiple sclerosis. *J Proteomics*. 2019;204:103403.

40. Catitti G, Cufaro MC, De Bellis D, et al. Extracellular vesicles in regenerative processes associated with muscle injury recovery of professional athletes undergoing sub maximal strength rehabilitation. *Int J Mol Sci*. 2022;23(23):14913.

41. Dykes JH, Toporski J, Juliusson G, et al. Rapid and effective CD3 T-cell depletion with a magnetic cell sorting program to produce peripheral blood progenitor cell products for haploidentical transplantation in children and adults. *Transfusion*. 2007;47(11):2134-2142.

42. Jafarinia M, Alsahebfosoul F, Salehi H, Eskandari N, Ganjalikhani-Hakemi M. Mesenchymal stem cell-derived extracellular vesicles: a novel cell-free therapy. *Immunol Invest*. 2020;49(7):758-780.

43. De Matteis S, Dicataldo M, Casadei B, et al. Peripheral blood cellular profile at pre-lymphodepletion is associated with CD19-targeted CAR-T cell-associated neurotoxicity. *Front Immunol*. 2022;13:1058126.

44. Wang X, Zhang Y, Wang S, et al. The role of CXCR3 and its ligands in cancer. *Front Oncol*. 2022;12:1022688.

45. Bunse M, Pfeilschifter J, Bluhm J, et al. CXCR5 CAR-T cells simultaneously target B cell non-Hodgkin's lymphoma and tumor-supportive follicular T helper cells. *Nat Commun*. 2021;12(1):240.

46. Frose J, Rowley J, Farid AS, et al. Development of an antigen-based approach to noninvasively image CAR T cells in real time and as a predictive tool. *Sci Adv*. 2024;10(38):eadn3816.

47. Lee SH, Soh H, Chung JH, et al. Feasibility of real-time in vivo 89Zr-DFO-labeled CAR T-cell trafficking using PET imaging. *PLoS One*. 2020;15(1):e0223814.

48. Ho JY, Wang L, Liu Y, et al. Promoter usage regulating the surface density of CAR molecules may modulate the kinetics of CAR-T cells in vivo. *Mol Ther Methods Clin Dev*. 2021;21:237-246.

49. Sadallah S, Eken C, Martin PJ, Schifferli JA. Microparticles (ectosomes) shed by stored human platelets downregulate macrophages and modify the development of dendritic cells. *J Immunol*. 2011;186(11):6543-6552.

50. Wu Y, Liu Y, Huang Z, et al. Control of the activity of CAR-T cells within tumours via focused ultrasound. *Nat Biomed Eng*. 2021;5(11):1336-1347.

51. Radler J, Gupta D, Zickler A, Andaloussi SE. Exploiting the biogenesis of extracellular vesicles for bioengineering and therapeutic cargo loading. *Mol Ther*. 2023;31(5):1231-1250.

52. Zara M, Guidetti GF, Camera M, et al. Biology and role of extracellular vesicles (EVs) in the pathogenesis of thrombosis. *Int J Mol Sci*. 2019;20(11):2840.

53. Blanchard N, Lankar D, Faure F, et al. TCR activation of human T cells induces the production of exosomes bearing the TCR/CD3/zeta complex. *J Immunol*. 2002;168(7):3235-3241.

54. Beider K, Itzhaki O, Schachter J, et al. Molecular and functional signatures associated with CAR T cell exhaustion and impaired clinical response in patients with B cell malignancies. *Cells*. 2022;11(7):1140.

55. Garcia-Calderon CB, Sierro-Martinez B, Garcia-Guerrero E, et al. Monitoring of kinetics and exhaustion markers of circulating CAR-T cells as early predictive factors in patients with B-cell malignancies. *Front Immunol*. 2023;14:1152498.

56. Danesh A, Inglis HC, Jackman RP, et al. Exosomes from red blood cell units bind to monocytes and induce proinflammatory cytokines, boosting T-cell responses in vitro. *Blood*. 2014;123(5):687-696.

57. Dinkla S, van Cranenbroek B, van der Heijden WA, et al. Platelet microparticles inhibit IL-17 production by regulatory T cells through P-selectin. *Blood*. 2016;127(16):1976-1986.

58. Pinheiro MK, Tamagne M, Elayeb R, Andrieu M, Pirenne F, Vingert B. Blood microparticles are a component of immune modulation in red blood cell transfusion. *Eur J Immunol*. 2020;50(8):1237-1240.

59. Neyrinck-Leglantier D, Tamagne M, L'Honore S, et al. Autologous blood extracellular vesicles and specific CD4(+) T-cell co-activation. *Front Immunol*. 2022;13:992483.

60. Cagnet L, Neyrinck-Leglantier D, Tamagne M, et al. CD27(+) microparticle interactions and immunoregulation of CD4(+) T lymphocytes. *Front Immunol*. 2023;14:1043255.

61. Sadallah S, Amicarella F, Eken C, Iezzi G, Schifferli JA. Ectosomes released by platelets induce differentiation of CD4+T cells into T regulatory cells. *Thromb Haemost*. 2014;112(6):1219-1229.

62. Dang XTT, Kavishka JM, Zhang DX, Pirisinu M, Le MTN. Extracellular vesicles as an efficient and versatile system for drug delivery. *Cells*. 2020;9(10):2191.

63. Zhang X, Jiang Y, Huang Q, et al. Exosomes derived from adipose-derived stem cells overexpressing glyoxalase-1 protect endothelial cells and enhance angiogenesis in type 2 diabetic mice with limb ischemia. *Stem Cell Res Ther*. 2021;12(1):403.

64. Dong L, Feng M, Kuczler MD, et al. Tumour tissue-derived small extracellular vesicles reflect molecular subtypes of bladder cancer. *J Extracell Vesicles*. 2024;13(2):e12402.

65. Giacobino C, Canta M, Fornaguera C, Borros S, Cauda V. Extracellular vesicles and their current role in cancer immunotherapy. *Cancers (Basel)*. 2021;13(9):2280.